

AdaAfford: Learning to Adapt Manipulation Affordance for 3D Articulated Objects via Few-shot Interactions

Yian Wang*
CFCS, CS Dept., PKU
AIIT, PKU
yianwang@pku.edu.cn

Ruihai Wu*
CFCS, CS Dept., PKU
AIIT, PKU
wuruihai@pku.edu.cn

Kaichun Mo*
Stanford University
kaichun@cs.stanford.edu

Jiaqi Ke
CFCS, CS Dept., PKU
AIIT, PKU
kjq001220@pku.edu.cn

Qingnan Fan
Tencent AI Lab
fqnchina@gmail.com

Leonidas Guibas
Stanford University
guibas@cs.stanford.edu

Hao Dong†
CFCS, CS Dept., PKU
AIIT, PKU
Peng Cheng Lab
hao.dong@pku.edu.cn

<https://hyperplane-lab.github.io/AdaAfford>

Abstract

Perceiving and interacting with 3D articulated objects, such as cabinets, doors, and faucets, pose particular challenges for future home-assistant robots performing daily tasks in human environments. Besides parsing the articulated parts and joint parameters, researchers recently advocate learning manipulation affordance over the input shape geometry which is more task-aware and geometrically fine-grained. However, taking only passive observations as inputs, these methods ignore many hidden but important kinematic constraints (e.g., joint location and limits) and dynamic factors (e.g., joint friction and restitution), therefore losing significant accuracy for test cases with such uncertainties. In this paper, we propose a novel framework, named AdaAfford, that learns to perform very few test-time interactions for quickly adapting the affordance priors to more accurate instance-specific posteriors. We conduct large-scale experiments using the PartNet-Mobility dataset and prove that our system performs better than baselines.

1. Introduction

For future home-assistant robots to aid humans in accomplishing diverse everyday tasks, we must equip them with strong capabilities perceiving and interacting with diverse 3D objects in human environments. Articulated objects, such as cabinets, doors, and faucets, are particularly interesting kinds of 3D shapes in our daily lives since agents can interact with them and trigger functionally important state changes of the objects (e.g., push closed the drawer of the cabinet, rotate the handle and pull open the door, turn on/off the water from the faucet by rotating the switch). However, because robots need to understand more semantically complicated part semantics and manipulate articulated parts with higher degree-of-freedom than rigid objects, it remains a very important yet challenging task to perceive and interact with 3D articulated objects.

Many previous works have investigated the problem of perceiving and interacting with 3D articulated objects. Researchers have been pushing the state-of-the-arts on segmenting articulated parts [31, 40], tracking them [29, 34], and estimating joint parameters [33, 38], which enable robotic systems [2, 22, 32] to successfully perform sophisticated planning and control over 3D articulated objects.

More recently, beyond recognizing the articulated parts and joints, researchers have been proposing learning more task-aware and geometrically fine-grained manipulation af-

*Equal contribution

†Corresponding author

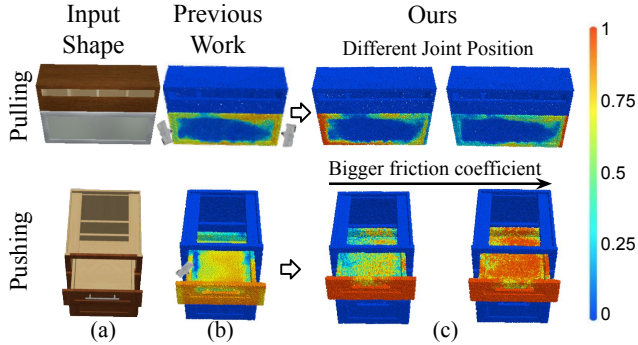


Figure 1. For robotic manipulation over 3D articulated objects such as pulling open a cabinet door or pushing closed a drawer (a), past works [17, 35] have demonstrated the usefulness of predicting per-point densely labeled manipulation affordance (b). However, only observing static visual inputs passively, these systems suffer from intrinsic ambiguities over kinematic constraints (e.g., location of the door axis in the top example) and dynamic properties (e.g., part joint friction in the bottom example). Our *AdaAfford* framework is able to perform very few test-time interactions to reduce such uncertainties and quickly adapt to predicting instance-specific affordance posteriors (c), where different door kinematic structures for the top-row cabinets are figured out and varying dynamic parameters of the drawer render changing affordance predictions in the bottom row.

fordance over input 3D geometry. Where2Act [17], the most related to our work, learns densely labeled manipulation affordance heatmaps over 3D input partial scans of articulated objects, as illustrated in Fig. 1 (b), by performing self-supervised trial-and-error interaction in a physical simulator. There are also many other works leveraging similar dense affordance predictions over 3D scenes [20] and rigid objects [16].

Such densely labeled affordance predictions over 3D data provide more geometrically fine-grained actionable information and can be learned task-specifically given different manipulation actions, showing promises in bridging the perception-interaction gaps for robotic manipulation over large-scale 3D data across different tasks.

However, taking only a single-frame observation of the 3D shape as input (e.g., a single 2D image, a single partial 3D scan), these methods systematically fail to capture many hidden but important kinematic or dynamic factors and therefore predict inaccurate affordance heatmaps, similar to Fig. 1 (b), by averaging out such uncertainties.

For example, given a cabinet with a fully closed door and no obvious door handle as shown in Fig. 1 (top-row), it is uncertain if the door axis is on the left or right side, which significantly affects the manipulation affordance predictions. Other kinematic uncertainties include joint limits (e.g., push inward or pull outward for a door) and types (e.g., slide or rotate to open a door).

Besides, various dynamic or physical parameters (e.g.,

the part mass, the joint friction) are also unobservable from single-frame inputs but largely affect manipulation affordance. For example, with increasing friction coefficient for a cabinet drawer (Fig. 1, bottom-row), robots would be able to push the inner board.

In this paper, we propose a novel framework *AdaAfford* which learns to perform very few test-time interactions to reduce such kinematic or dynamic uncertainties and fastly adapts the affordance prior predictions to instance-specific posteriors given a novel test shape. Our system learns a *data-efficient strategy* that sequentially samples very few uncertain or interesting locations to interact, as the interacting grippers illustrated in Fig. 1 (b), according to the current affordance predictions and past interaction trials (we begin with the affordance prior predictions of Where2Act [17] and zero interaction history). The interaction outcomes, each of which includes the interaction location, direction, and the resulting part motion, are then observed and incorporated to produce posterior affordance predictions, as illustrated in Fig. 1 (c), by a proposed *fast-adaptation mechanism*.

We set up a benchmark for experiments and evaluations using the large-scale PartNet-Mobility dataset [19] and the SAPIEN physical simulator [36]. We use in total 972 shapes from 15 object categories and conduct experiments for several action types and experiment settings. We randomly sample the kinematic and dynamic parameters for the 3D articulated objects in simulation to support the study.

Experiments show that our method can successfully and efficiently adapt manipulation affordance to novel test shapes with as few as one to four interactions. Quantitative comparisons to baselines further prove the effectiveness of our proposed approach.

In summary, our main contributions are the following.

- we point out and investigate an important limitation of the methods that learn densely labeled visual manipulation affordance – the unawareness of hidden yet important kinematic and dynamic uncertainties;
- we propose a novel framework *AdaAfford* that learns to perform very few test-time interactions to reduce uncertainties and quickly adapt to predicting an instance-specific affordance posterior;
- we set up a large-scale benchmark, built upon PartNet-Mobility [19] and SAPIEN [36], for experiments and evaluations, and results demonstrated the effectiveness and efficiency of the proposed approach.

2. Related Work

Visual Affordance on 3D Shapes. Affordance [9] suggests possible ways for agents to interact with objects. Many past works have investigated learning grasp [12, 14, 25, 28] and manipulation [16, 17, 20, 26, 35] affordance for robot-object interaction, while there are also works studying affordance for hand-object [3, 4, 11, 16, 39], object-

object [18, 30, 44], and human-scene [8, 15, 20, 24] interaction scenarios.

Among these works, researchers have proposed different representations for visual affordance, including detection locations [14, 28], parts [16], keypoints [26], heatmaps [17, 20], etc. In this work, we mostly follow the settings in [17] for learning visual affordance heatmaps for manipulating 3D articulated objects. Different from previous works that infer possible agent-object visual affordance heatmaps passively from static visual observations, our framework leverages active interactions to efficiently query uncertain kinematic or dynamic factors for learning more accurate instance-adaptive visual affordance.

Fast Adaption via Few-shot Interactions. Researchers have explored various approaches [5, 7, 27, 42, 43] for fast adaption via few-shot interactions. Many past works have also designed interactive perception methods to figure out object mass [13], dynamic parameters [1, 6, 10, 37], or parameters for known models [41]. Different from these studies proposing general algorithms for policy adaptation or figuring out explicit system parameters for rigid objects, we focus on designing a working solution for our specific task of learning visual affordance heatmaps for manipulating 3D articulated objects with special designs on predicting geometry-grounded interaction proposals and interaction-adaptive affordance predictions.

3. Problem Formulation

Given as input a single-frame 3D partial point cloud observation of an articulated object $O \in \mathbb{R}^{N \times 3}$ (e.g., lifted from a depth scanner with known camera intrinsics), the Where2Act framework [17] directly outputs a densely labeled per-point manipulation affordance heatmap $A \in [0, 1]^N$, where higher scores indicate bigger chances for being interacted with to accomplish a given short-term manipulation task (e.g., pushing, pulling). Additionally, a diverse set of gripper orientations $\{R_1^p, R_2^p, \dots | R_i^p \in SO(3)\}$ is proposed at each point $p \in O$ suggesting possible ways for robot agents to interact with the point, each of which is also associated with a success likelihood $s_i^p \in [0, 1]$. No interaction is allowed at the test time in Where2Act and a fixed set of system dynamic parameters is used across all the shapes.

We follow most of the Where2Act settings except that we randomly vary the system dynamics and allow test-time interactions over the 3D shape to reduce kinematic or dynamic uncertainties. Our AdaAfford system proposes a few interactions sequentially $\mathcal{I} = \{I_1, I_2, \dots\}$. Each interaction $I_i = (O_i, p_i, R_i, m_i)$ executes a task-specific hard-coded short-term trajectory defined in Where2Act, parametrized by the interaction point $p_i \in O_i$ and the gripper orientation $R_i \in SO(3)$, and observes a part motion m_i . Starting from the input shape observation $O_1 \leftarrow O$, every interaction I_i where $m_i \neq 0$ changes the part state

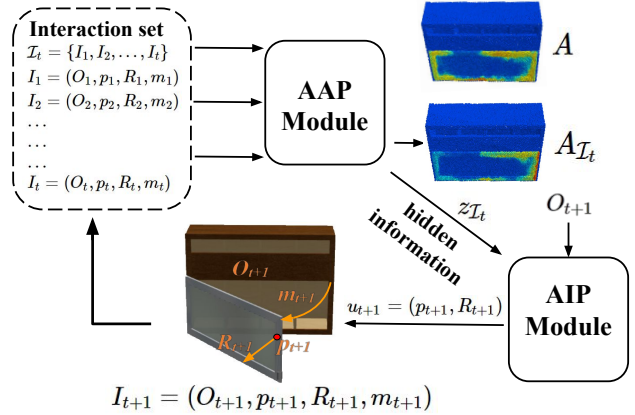


Figure 2. **Method Overview.** Starting from the Where2Act [17] predicted affordance prior A , at each timestep $t = 1, 2, \dots$, we recursively leverage the *Adaptive Interaction Proposal* (AIP) module to propose a next-time interaction action u_{t+1} including an interaction position p_{t+1} and a gripper orientation R_{t+1} , observe the interaction outcome m_{t+1} , and feed through the *Adaptive Affordance Prediction* (AAP) module all past few-shot interactions \mathcal{I}_t together with the new one I_{t+1} for adapting to an affordance posterior prediction $A_{\mathcal{I}_{t+1}}$. The procedure iterates until the interaction budget is reached or the AIP module decides to stop.

and thus produces a new shape point cloud input for the next interaction $O_{i+1} \neq O_i$. Leveraging the interaction observations \mathcal{I} , our system then adapts the per-point manipulation affordance A predicted by Where2Act to a posterior $A_{\mathcal{I}} \in [0, 1]^N$ that reduces uncertainties and provides more accurate instance-specific predictions. For each gripper orientation R_i , we also update the success likelihood score $s_{i,\mathcal{I}}^p \in [0, 1]$ considering the test-time interactions.

4. Method

Our proposed *AdaAfford* framework primarily consists of two modules – an *Adaptive Interaction Proposal* (AIP) module and an *Adaptive Affordance Prediction* (AAP) module.

While the AIP module learns a greedy yet effective strategy for sequentially proposing the few-shot test-time interactions $\mathcal{I} = \{I_1, I_2, \dots\}$, the AAP module is trained to adapt the affordance predictions from the Where2Act [17] prior A to a posterior $A_{\mathcal{I}}$ observing the sampled interactions \mathcal{I} .

We iterate the two modules recurrently at the test time to produce a sequence of few-shot interactions \mathcal{I} leading to the final affordance posterior prediction $A_{\mathcal{I}}$. During training, we iteratively alternate the training for the two modules until a joint convergence.

Below, we first introduce the test-time inference procedure for a brief overview. Next, we describe the input backbone encoders that are shared among all networks in our framework. Then, we describe the detailed architectures

and system designs of the two modules. We conclude with the training losses and strategy.

Test-time Overview. Fig. 2 presents an overview of the method. We apply a recurrent structure at test time. Starting from the affordance prediction A without any interaction, the AIP module proposes the first action for producing the interaction data I_1 . Then, at each timestep $t = 1, 2, \dots$, we feed the current set of interactions $\mathcal{I}_t = \{I_1, \dots, I_t\}$ as inputs to the AAP module and extract hidden information $z_{\mathcal{I}_t} \in \mathbb{R}^{32}$ that adapts the affordance map prediction to $A_{\mathcal{I}_t}$. The AIP module then takes $z_{\mathcal{I}_t}$ as input and proposes an action $u_{t+1} = (p_{t+1}, R_{t+1})$ composed of the interaction point p_{t+1} and the gripper orientation R_{t+1} for the next interaction. Performing this action in the environment, we obtain the next-step interaction data $I_{t+1} = (O_{t+1}, p_{t+1}, R_{t+1}, m_{t+1})$ and put it into the interaction set $\mathcal{I}_{t+1} \leftarrow \mathcal{I}_t \cup \{I_{t+1}\}$. We iterate until the interaction budget has been reached or our AIP module decides to stop. When the procedure stops at timestep T , we output the final affordance posterior $A_{\mathcal{I}} = A_{\mathcal{I}_T}$.

Input Encoders. This paragraph details how we encode inputs into features as all the encoder networks in the two modules take the same input entities (e.g., the shape observation O , the interaction action u) and thus share the same architecture. We use the PointNet++ segmentation network [23] to encode the input shape point cloud $O \in \mathbb{R}^{N \times 3}$ into per-point feature maps $f_O \in \mathbb{R}^{N \times 128}$ and denote $f_{p|O} \in \mathbb{R}^{128}$ as the feature at any point $p \in O$. We use Multilayer Perceptron (MLP) networks to encode other vector inputs (e.g., the interaction action u) into $f_* \in \mathbb{R}^{128}$ (e.g., f_u). In the following subsections, when receiving inputs, the networks in our framework will first encode them into $f_{p|O}$ and f_* , and then concatenate them into $f_I \in \mathbb{R}^{256}$. The encoders do not share weights across different modules.

4.1. Adaptive Affordance Prediction Module

The *Adaptive Affordance Prediction* (AAP) module takes as inputs few-shot interactions \mathcal{I} and predicts the affordance posterior $A_{\mathcal{I}}$.

This module is composed of three subnetworks: 1) an *Adaptive Information Encoder* \mathcal{E}_{AAP} that extracts hidden information $z \in \mathbb{R}^{32}$ from a set of interactions \mathcal{I} ; 2) an *Adaptive Affordance Network* \mathcal{D}_{AAP} that predicts the posterior affordance heatmap $A_{\mathcal{I}}$ conditioned on the hidden information z ; and 3) an *Adaptive Critic Network* \mathcal{C}_{AAP} that predicts the AAP action score $s_{u|z}^{AAP} \in [0, 1]$ for an action u conditioned on the hidden information z . Here, an action is represented as $u = (p, R)$ including an interaction point $p \in O$ and a gripper orientation $R \in SO(3)$.

Adaptive Information Encoder. Given a set of interactions $\mathcal{I} = \{I_1, I_2, \dots\}$ as input, the *Adaptive Information*

Encoder \mathcal{E}_{AAP} outputs a 32-dim hidden information representation $z_{\mathcal{I}}$ (z for brevity). It first encodes each interaction I_i using the input encoders mentioned before, and then uses an MLP network to encode the features into a 32-dim latent code z_{I_i} representing the hidden information extracted from I_i . As different interactions contain different amount of hidden information, we use another MLP Network to predict an attention score w_{I_i} for each interaction. To get a summarized hidden information from a set of Interactions, we simply computes a weighted average over all z_{I_i} 's according to the weights w_{I_i} 's and use the resulting feature as $z_{\mathcal{I}}$. Formally, we have $z_{\mathcal{I}} \leftarrow (\sum_i z_{I_i} \times w_{I_i}) / (\sum_i w_{I_i})$.

Adaptive Critic Network. Given the object partial point cloud observation O , an arbitrary interaction point $p \in O$, an arbitrary gripper orientation $R \in SO(3)$ and the latent code z which contains the extracted hidden information, the *Adaptive Critic Network* \mathcal{C}_{AAP} predicts an AAP action score $s_{u|z}^{AAP} \in [0, 1]$ indicating the likelihood for the success of the interaction action u given the interaction information z . It first encodes the input $\{O, p, R\}$ using the input encoders as mentioned before and then employs an MLP network that takes the concatenated features together with z as inputs and predicts an AAP action score $s_{u|z}^{AAP}$ as the output. A higher AAP action score $s_{u|z}^{AAP}$ for an action u indicates a higher chance for u to succeed in accomplishing the given manipulation task.

Adaptive Affordance Network. Given the input object partial point cloud O , an arbitrary point $p \in O$, and the latent code z which contains hidden information, the *Adaptive Affordance Network* \mathcal{D}_{AAP} predicts an actionability score $a_{p|z}^{AAP} \in [0, 1]$ at the point p . It first encodes the input $\{O, p\}$ using the aforementioned input encoders and then uses an MLP network that takes the concatenated features together with z as inputs and produces an actionability score $a_{p|z}^{AAP}$ as the output. A higher actionability score $a_{p|z}^{AAP}$ indicates a higher chance for the gripper to successfully interact on the point p .

4.2. Adaptive Interaction Proposal Module

The *Adaptive Interaction Proposal* (AIP) module proposes an action $u_{t+1} = (p_{t+1}, R_{t+1})$ for the next step interaction (denote the current timestep as t) given the feature z extracted from the current interaction observations \mathcal{I} . This module is composed of two networks: 1) an *Adaptive Interaction Proposal Affordance Network* \mathcal{D}_{AIP} that predicts an AIP actionability score $a_{p|z}^{AIP} \in \mathbb{R}$ indicating how likely the next-action is worth interacting at point p , and 2) an *Adaptive Interaction Proposal Critic Network* \mathcal{C}_{AIP} predicting an AIP action score $s_{u|z}^{AIP} \in \mathbb{R}$ for an action u suggesting what gripper orientation to pick for the next interaction. We leverage the predictions of the two networks to propose the next interaction action $u_{t+1} = (p_{t+1}, R_{t+1})$.

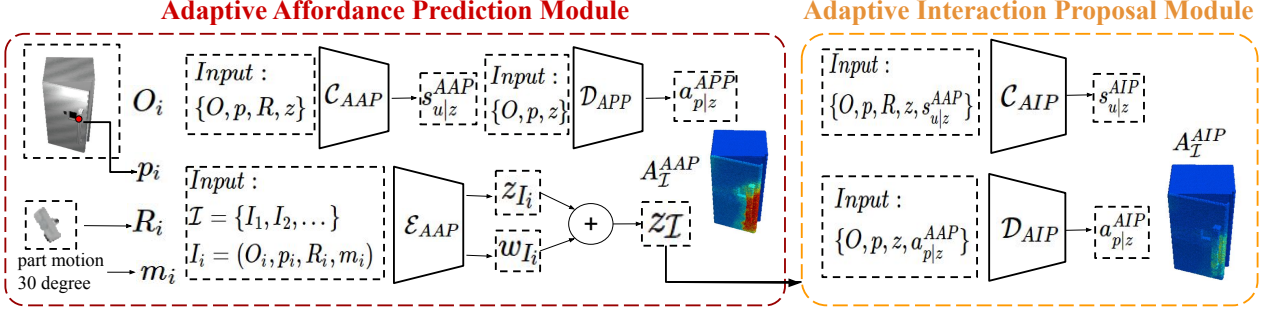


Figure 3. **Network Architecture.** Left: the *Adaptive Affordance Prediction* (AAP) module takes as inputs the few-shot interactions \mathcal{I} and predicts the affordance posterior $A_{\mathcal{I}}$. It has three subnetworks: an *Adaptive Information Encoder* \mathcal{E}_{AAP} that computes a weighted average over features of the current interaction observations \mathcal{I} and extracts a latent instance-adaptive information $z_{\mathcal{I}}$ (z for brevity), an *Adaptive Critic Network* \mathcal{C}_{AAP} that estimates success likelihood $s_{u|z}^{AAP}$ for an arbitrary action $u = (p, R)$ conditioned on $z_{\mathcal{I}}$, and an *Adaptive Affordance Network* \mathcal{D}_{AAP} that predicts the actionable affordance posterior $a_{p|z}^{AAP} \in A_{\mathcal{I}}^{AAP}$ over every location $p \in O$ given $z_{\mathcal{I}}$. Right: the *Adaptive Interaction Proposal* (AIP) module proposes a next-step interaction action $u_{t+1} = (p_{t+1}, R_{t+1})$ (denote the current timestep as t) given the feature $z_{\mathcal{I}}$ extracted from the current interaction observations \mathcal{I} . There are two subnetworks: an *AIP Critic Network* \mathcal{C}_{AIP} that rates a next-action likelihood $s_{u|z}^{AIP}$ for an arbitrary action $u = (p, R)$ and an *AIP Affordance Network* \mathcal{D}_{AIP} that assigns a next-action chance $a_{p|z}^{AIP}$ for every point p . At the test time, one can first sample a point p_{t+1} worth trying for the next interaction from the predicted heatmap $A_{\mathcal{I}}^{AIP}$ and then pick a gripper orientation R_{t+1} using the action ratings $s_{u|z}^{AIP}$'s.

Adaptive Interaction Proposal Critic Network. Given the input object partial point cloud O , an arbitrary interaction point $p \in O$, an arbitrary gripper orientation $R \in SO(3)$, the latent code z which contains hidden information, and the AAP action score $s_{u|z}^{AAP}$ produced by \mathcal{C}_{AAP} , the *AIP Critic Network* \mathcal{C}_{AIP} predicts the AIP action score $s_{u|z}^{AIP} \in \mathbb{R}$ of u . It first encodes the inputs $\{O, p, R, s_{u|z}^{AAP}\}$ using the input encoders and then uses an MLP network that takes the concatenated features together with z as inputs and generates an AIP action score $s_{u|z}^{AIP}$ for the action u . A higher AIP action score suggests that the action u may query more unknown yet interesting hidden information and thus is worth exploring next.

Adaptive Interaction Proposal Affordance Network. Given the input partial shape observation O , an arbitrary interaction point $p \in O$, the latent code z which contains hidden information, and the AAP actionability score $a_{p|z}^{AAP}$ at point p estimated by \mathcal{D}_{AAP} , the *AIP Affordance Network* \mathcal{D}_{AIP} predicts the AIP actionability score $a_{p|z}^{AIP} \in \mathbb{R}$ at point p . It first encodes the inputs $\{O, p, a_{p|z}^{AAP}\}$ using the aforementioned input encoders and then employs an MLP network that takes the concatenated features together with z as inputs and predicts an AIP actionability score $a_{p|z}^{AIP}$. A higher AIP actionability score at p indicates that some unknown yet interesting hidden information may be obtained by executing an interaction at p which may further help the AAP module predict better actionable information.

Next-step Interaction Action Proposal. To propose an action $u_{t+1} = (p_{t+1}, R_{t+1})$ for the next interaction, given the hidden information z and the input shape partial point

cloud O , we first obtain the AIP actionability heatmap $A_{p|z}^{AIP}$ for every point $p \in O$ predicted by the *AIP Affordance Network* \mathcal{D}_{AIP} and then select the point $p_{t+1} \leftarrow p_*$ with the highest AIP actionability score $a_{p_*|z}^{AIP}$. Then, we sample 100 random actions $\{u_1, u_2, \dots, u_{100}\}$ at p using the Where2Act's pre-trained *Action Proposal Network*, use our *AIP critic network* \mathcal{C}_{AIP} to generate the AIP action scores $s_{u_i|z}^{AIP}$ for each action u_i , and then choose the action $u_{t+1} \leftarrow u_*$ with the highest AIP action score $s_{u_*|z}^{AIP}$.

Stopping Criterion for the Few-shot Interactions. The AIP procedure for generating few-shot interactions stops when a preset budget is reached or the maximal AIP actionability score is below a certain threshold (e.g., 0.05).

4.3. Training and Losses

Below, we describe the loss for training each of the subnetworks and the training strategy for the two modules.

AAP Action Scoring Loss. To supervise the *Adaptive Critic Network* \mathcal{C}_{AAP} , we use a standard binary cross entropy loss, which measures the error between the prediction of \mathcal{C}_{AAP} and target part's ground truth motion m of an interaction I . Specifically, given the hidden information z , a batch of interaction observations $\mathcal{I} = \{I_1, I_2, \dots, I_B\}$ where $I_i = \{O_i, u_i, m_i\}$, and the AAP action score prediction $s_{u_i|z}^{AAP}$ for each interaction I_i , the loss is defined as

$$\mathcal{L}_C^{AAP} = -\frac{1}{B} \sum_i r_i \log(s_{u_i|z}^{AAP}) + (1 - r_i) \log(1 - s_{u_i|z}^{AAP})$$

where $r_i = 1$ if $m_i > \tau$ (e.g., $\tau = 0.01$) or $r_i = 0$ rendering a binary discretization for each interaction outcome.

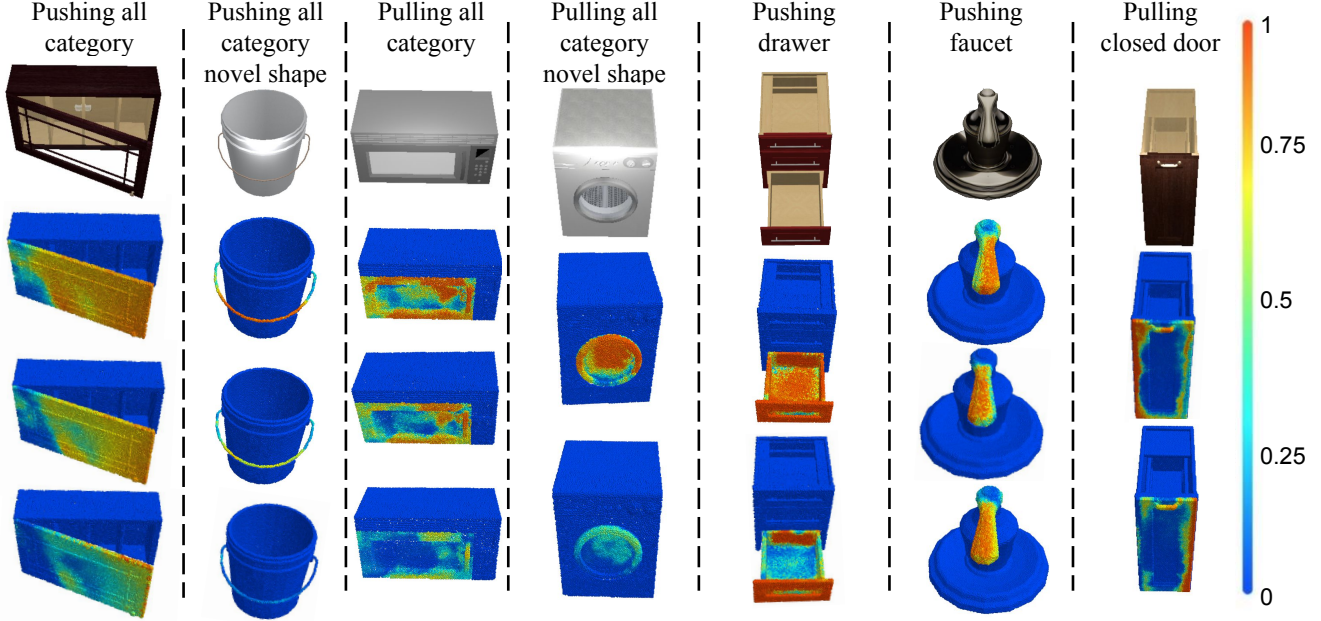


Figure 4. We visualize some example results for the adapted affordance predictions given by the AAP module conditioned on different hidden kinematic and dynamic information. The first five columns show the adapted affordance prediction conditioned on increasing joint friction (the first and second columns), part mass (the third column), and friction coefficient on the object surface (the fourth and fifth columns). The last two columns respectively show the influence of faucet handle’s different rotating directions (*i.e.*, joint limits) and the joint axis locations. Our AAP module can successfully adapt to the hidden instance-specific properties given few-shot interactions.

AAP Actionability Scoring Loss. To train the *Adaptive Affordance Network* \mathcal{D}_{AAP} , we use an \mathcal{L}_1 loss to measure the difference from the predicted score $a_{p|z}^{AAP}$ to the ground truth. To estimate the ground truth score for p , we randomly sample 100 actions at p according to the pre-trained Where2Act *Action Proposal Network*, predict the AAP action scores $s_{u|z}^{AAP}$ ’s of these actions u ’s using our \mathcal{C}_{APP} , and use the average of the top-5 scores.

AIP Action Scoring Loss. To supervise the *AIP Critic Network* \mathcal{C}_{AIP} , we use an \mathcal{L}_1 loss to measure the difference between our predicted AIP action score $s_{u|z}^{AIP}$ and the ground truth AIP action score $gt_{u|z}^{AIP}$. We design a greedy yet effective way to estimate the ground-truth scores. Given a set of interactions $\mathcal{I}_T = \{I_1, I_2, \dots\}$, to generate $gt_{u_i|z}^{AIP}$ for an interaction action u_i , we respectively encode two interaction subsets $\mathcal{I}_{i-1} = \{I_1, I_2, \dots, I_{i-1}\}$ and $\mathcal{I}_i = \{I_1, I_2, \dots, I_i\}$ into latent codes $z_{\mathcal{I}_i}$ and $z_{\mathcal{I}_{i-1}}$. Then, we feed $z_{\mathcal{I}_i}$ and $z_{\mathcal{I}_{i-1}}$ as the conditional inputs to the *Adaptive Critic Network* \mathcal{C}_{AAP} separately and count the difference of the AAP action scoring loss \mathcal{L}_C^{AAP} as the ground truth of AIP action score $gt_{u_i|z_{\mathcal{I}_{i-1}}}^{AIP}$. More concretely, let the AAP action scoring loss conditioned on $z_{\mathcal{I}_i}$ and $z_{\mathcal{I}_{i-1}}$ respectively be $\mathcal{L}_{\mathcal{I}_i}$ and $\mathcal{L}_{\mathcal{I}_{i-1}}$. We define the ground truth AIP action score $gt_{u_i|z_{\mathcal{I}_{i-1}}}^{AIP} \leftarrow \mathcal{L}_{\mathcal{I}_{i-1}} - \mathcal{L}_{\mathcal{I}_i}$. The AIP action score is trained to regress an estimated positive influence of executing u on the AAP action score predictions, where an

action giving more influence is preferred as it helps discover more hidden information useful to the task.

AIP Actionability Scoring Loss. To train the *AIP Affordance Network* \mathcal{D}_{AIP} , we use another \mathcal{L}_1 loss. For each position $p \in O$, we sample 100 actions u_i ’s using the pre-trained Where2Act *Action Proposal Network*, obtain the AIP action scores $s_{u_i|z}^{AIP}$ ’s of these actions u_i ’s predicted by the *AIP Critic Network* \mathcal{C}_{AIP} , and use the average of the top-5 scores as the regression target.

Training Strategy. We iteratively train the AAP module and AIP module until a joint convergence since the update of the subnetworks in one module will affect the training of the subnetworks in the other module.

More specifically, the update of \mathcal{C}_{AAP} and \mathcal{D}_{AAP} in the AAP module will affect the ground-truth AIP action scores, while the update of \mathcal{C}_{AIP} and \mathcal{D}_{AIP} in the AIP module will change the proposed interactions used to generate z in the AAP module. Therefore, our final solution is to train the AAP and AIP modules iteratively. The procedure starts with firstly training the AAP module using randomly sampled interactions. We then train the AIP module to learn to propose more efficient and effective proposals. Then, with the trained subnetworks in the AIP module, we finetune the AAP module with the proposed interactions. We iteratively alternate the training until both modules converge.

5. Experiments

We perform experiments using the large-scale PartNet-Mobility dataset [19] and the SAPIEN physical simulator [36] under different settings. We set up two baselines for comparisons. Results demonstrate the effectiveness and superiority of the proposed approach.

5.1. Data and Settings

Below, we describe the data, experiment settings, and environment settings we use in details.

Data. Following the settings of Where2Act [17], we conduct our experiments in the SAPIEN [36] simulator equipped with NVIDIA PhysX [21] simulation engine and the large scale PartNet-Mobility [19] dataset. We use 972 articulated 3D objects covering 15 object categories, mostly following Where2Act, to carry out the experiments. The dataset is divided into 10 training categories and 5 testing categories. The shapes in the training categories are further divided into two disjoint sets of training and test shapes. See supplementary for the detailed statistics.

Experiment Settings. Firstly, following Where2Act [17], we perform experiments over all object categories under different manipulation action types. We train one network for each downstream manipulation task over training shapes from the 10 training object categories and evaluate the performance over test shapes from the training categories and shapes from unseen test categories.

Besides, to further demonstrate the effectiveness of our method, we conduct two additional experiments under two challenging tasks with clear kinematic ambiguity, each of which is conducted over a single object category:

- pulling closed doors of cabinets that cannot be easily distinguished which side to pull open;
- pushing faucets with uncertainties which direction to rotate (clock-wise or counter-clock-wise).

These two experiments are particularly interesting yet challenging cases on which the previous work Where2Act [17] failed drastically and we hope to test our framework.

Environment Settings. Following Where2Act, we abstract away the robot arm and only use a Franka Panda flying gripper as the robot actuator. The input shape point cloud is assumed to be cleanly segmented out. To generate the input partial point cloud scans, we mount an RGB-D camera with known intrinsic parameters 5-unit-length away pointing to the center of the target object.

To simulate manipulating shapes with uncertain dynamics, we randomly change the following three physical parameters in SAPIEN: 1) the friction of the target part joint, 2) the mass of the target part, and 3) the friction coefficient of the target part surface. For the "pulling closed door" task, we manually select the cabinets whose doors have no clear

		F-score (%)			Sample-Succ (%)		
pushing all (train cat.)	Where2Act	56.44			20.85		
	ours-random	69.09 / 69.45 / 72.28			29.86 / 28.65 / 25.27		
	ours-final	70.50 / 73.96 / 74.63			35.70 / 35.50 / 35.14		
pushing all (test cat.)	Where2Act	49.95			21.69		
	ours-random	57.71 / 55.35 / 53.47			29.09 / 31.04 / 32.08		
	ours-final	58.44 / 58.06 / 60.38			30.00 / 30.39 / 33.50		
pulling all (train cat.)	Where2Act	31.19			1.92		
	ours-random	28.58 / 24.40 / 15.09			3.89 / 3.33 / 3.89		
	ours-final	35.73 / 37.20 / 37.50			3.33 / 6.67 / 9.44		
pulling all (test cat.)	Where2Act	36.36			10.00		
	ours-random	15.09 / 44.32 / 38.24			8.70 / 4.78 / 10.00		
	ours-final	39.10 / 35.29 / 49.78			10.45 / 10.83 / 10.87		
pulling closed door	Where2Act	48.44			4.38		
	ours-random	51.37 / 57.67 / 64.96			7.41 / 9.13 / 9.56		
	ours-final	56.11 / 58.68 / 67.68			7.63 / 11.36 / 17.08		
pushing faucet	Where2Act	20.08			26.59		
	ours-random	76.60 / 76.08 / 77.98			35.46 / 35.57 / 39.25		
	ours-final	76.01 / 76.93 / 78.40			36.53 / 46.23 / 50.44		

Table 1. **Quantitative Evaluations and Comparisons.** We compare our method to two baseline methods: the Where2Act [17] approach that ignores the hidden information and the ours-random baseline that replaces the interaction candidates proposed by the AIP module with random ones. We experiment with three different test-time interaction budgets (*i.e.*, 1, 2, or 4) and report the numbers separated by slashes. We use "pushing all" and "pulling all" to denote the experiments over all object categories, while "pulling closed door" and "pushing faucet" refer to the experiments over a single category only. For the experiments over all categories, we report the performance over novel shapes from the training categories (marked with "train cat.") and shapes from novel categories (marked with "test cat."). We see clearly that ours-final achieves the best performance in most entries.

handle geometry in the PartNet-Mobility dataset [36], and set the poses of those doors to be closed. The gripper cannot tell which side to pull open the door because it is impossible to tell whether the axis position is on the left or right of the door from passive visual observations. For the "pushing faucet" task, we randomly set the rotating direction of the faucet switch to be in one of the following three modes: only clock-wise, only counter clock-wise, or both ways.

5.2. Baselines and Evaluation Metrics.

We set up two baseline methods and employ two evaluation metrics for quantitative comparisons.

Baseline Methods. We compare our framework with two baselines: 1) Where2Act [17], which manipulate the shape with pure visual information only (*i.e.*, without any interactions as input). 2) Ours-random that replaces the interaction candidates proposed by the AIP module with random ones. We compare to the Where2Act baseline to show that using few-shot interactions indeed helps improve the performance and use the ours-random baseline to show that strategically learning where and how to interact is important.

Notice that since the Where2Act baseline directly predicts the affordance map without performing interactions, there are inevitably uncertain cases that limit its performance. For the ours-random baseline, instead of using the

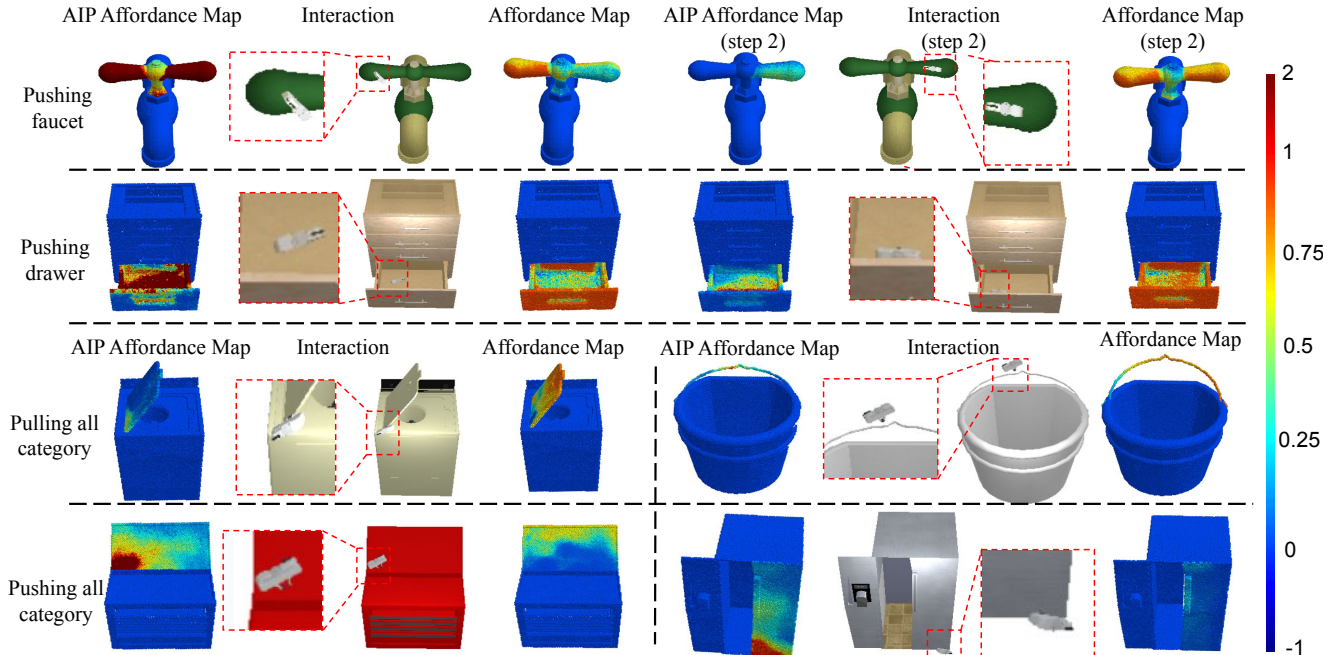


Figure 5. We visualize example results for the interactions proposed by the AIP module and the corresponding AIP affordance map predictions. In the first two rows, we show the initial and the second AIP affordance maps, the corresponding proposed interactions, and the posterior affordance map predictions. In the third and fourth rows, we present four more examples that only one interaction is needed. From these results, we observe that our AIP module successfully proposes reasonable interactions for querying useful hidden information.

interactions that the AIP module proposes, we randomly select contact points on the target part, sample 100 gripper orientations at each point using the pretrained Where2Act *Action Proposal Network*, obtain the AAP action scores of these actions, and finally pick the action with the highest score to execute at each point.

Evaluation Metrics. Following Where2Act [17], we use the F-score, balancing the precision and recall, to evaluate the predictions of the *Adaptive Critic Network* \mathcal{C}_{AAP} , and use the sample-successful rate (Sample-Succ) to evaluate the performance of the *Adaptive Critic Network* \mathcal{C}_{AAP} and the *Adaptive Affordance Network* \mathcal{D}_{AAP} . To compute the sample successful rate, we apply the learned test-time strategy to fill \mathcal{I} and then use the extracted hidden information z as the conditional input to \mathcal{C}_{AAP} and \mathcal{D}_{AAP} . After that, we randomly select a point to interact from the group of points with the top-100 actionability scores $a_{p|z}^{AAP}$, sample 100 actions u_i 's at p , obtain the AAP action scores $s_{u_i|z}^{AAP}$ of these actions u_i 's predicted by the AAP *Critic Network* \mathcal{C}_{AAP} , and then choose the action u_i with the highest $s_{u_i|z}^{AAP}$ to execute. We perform 10 interaction trials per test shape and report the final sample-succ rate as the percentage of sampling successful interactions in simulation.

5.3. Results and Analysis

We compare our method with the Where2Act baseline and the random baseline. The quantitative results in Ta-

ble 1 show that our method achieves the best performance in most comparison entries. Specifically, compared with Where2Act, our method with even only 1 interaction can improve the performance evidently. Also, the performance increases as the number of interactions increases. Comparing against the ours-random baseline, we further validate the usefulness of the AIP module. We see that our method can generalize well to novel shapes and even shapes from unseen object categories.

Figure 4 shows example visualizations for our predicted affordance map posterior given interactions under different hidden kinematic or dynamic information, including 1) the joint position of a closed door with no clear handle, 2) the rotating direction of a faucet handle, 3) the friction coefficient on object surface, 4) the friction of target object's joint, and 5) the mass of the target object. For example, in the first (second) column, we observe that with bigger joint friction coefficients the door (handle) is harder to manipulate and one needs to push (pull) at only points very far away from the joint axis to accomplish the task. On the right-most (second-to-the-right) column, our network successfully figures out which side of the door (faucet switch) one needs to push. From these figures, it is clear to see that our proposed method successfully adapts the affordance prediction conditioned on different hidden information.

Figure 5 further shows some interaction proposals by our AIP module with its influence on the prediction of AAP

affordance map and to the AIP affordance map itself. In the first row, for example, we see that the AIP affordance first proposes to interact at both sides of the faucet since it knows little about the hidden information but at the second timestep proposes the complementary side as it already learns that the left side is actionable. In the last two rows, we respectively show the "pulling all category" cases and "pushing all category" cases which only require one step to adapt. The cases on the left side and top-right show how our framework adapts to the part mass and joint friction uncertainties, while the bottom-right case shows how it recognizes that the closed door cannot be pushed. Plus, although our AIP actionability scores range in \mathbb{R} , we empirically find that our predicted AIP affordance maps contain no score lower than zero, demonstrating that our system learns as expected that performing more actions, though maybe not helpful, will not hurt the performance.

See supplementary for additional results and analysis.

6. Conclusion

This work addresses a big limitation of previous works learning visual actionable affordance for manipulating 3D articulated objects – the hidden kinematic or dynamic uncertainties. We propose a novel framework AdaAfford that samples a few test-time interactions for fastly adapting to a more accurate affordance posterior prediction removing such ambiguities. Experimental results validate the effectiveness of our method compared to baseline approaches.

Limitations and Future Works. This work only considers two action types and 3D articulated objects. Future works may study more interaction and data types. Also, we only perform short-term interactions and future works can investigate how to extend the framework for long-term manipulation trajectories. Finally, we abstract away the complexity of robot arms and only use flying grippers in our experiments to learn object-centric visual affordance. Future works shall work on considering the robot arm constraints.

7. Acknowledgement

This work was supported by National Natural Science Foundation of China —Youth Science Fund (No.62006006): Learning Visual Prediction of Interactive Physical Scenes using Unlabelled Videos.

References

- [1] Pulkit Agrawal, Ashvin Nair, Pieter Abbeel, Jitendra Malik, and Sergey Levine. Learning to poke by poking: Experiential learning of intuitive physics. *arXiv preprint arXiv:1606.07419*, 2016. 3
- [2] Sachin Chitta, Benjamin Cohen, and Maxim Likhachev. Planning for autonomous door opening with a mobile manipulator. In *2010 IEEE International Conference on Robotics and Automation*, pages 1799–1806. IEEE, 2010. 1
- [3] Enric Corona, Albert Pumarola, Guillem Alenya, Francesc Moreno-Noguer, and Grégory Rogez. Ganhand: Predicting human grasp affordances in multi-object scenes. In *Proceedings of the IEEE/CVF Conference on Computer Vision and Pattern Recognition*, pages 5031–5041, 2020. 2
- [4] Kuan Fang, Te-Lin Wu, Daniel Yang, Silvio Savarese, and Joseph J Lim. Demo2vec: Reasoning object affordances from online videos. In *Proceedings of the IEEE Conference on Computer Vision and Pattern Recognition*, pages 2139–2147, 2018. 2
- [5] Karim Farid and Nourhan Sakr. Few shot system identification for reinforcement learning. *arXiv preprint arXiv:2103.08850*, 2021. 3
- [6] Fabio Ferreira, Lin Shao, Tamim Asfour, and Jeannette Bohg. Learning visual dynamics models of rigid objects using relational inductive biases. *arXiv preprint arXiv:1909.03749*, 2019. 3
- [7] Chelsea Finn, Pieter Abbeel, and Sergey Levine. Model-agnostic meta-learning for fast adaptation of deep networks. In *International Conference on Machine Learning*, pages 1126–1135. PMLR, 2017. 3
- [8] David F Fouhey, Vincent Delaitre, Abhinav Gupta, Alexei A Efros, Ivan Laptev, and Josef Sivic. People watching: Human actions as a cue for single view geometry. In *European Conference on Computer Vision*, pages 732–745. Springer, 2012. 3
- [9] James J Gibson. The theory of affordances. *Hilldale, USA*, 1(2):67–82, 1977. 2
- [10] Michael Janner, Sergey Levine, William T Freeman, Joshua B Tenenbaum, Chelsea Finn, and Jiajun Wu. Reasoning about physical interactions with object-oriented prediction and planning. *arXiv preprint arXiv:1812.10972*, 2018. 3
- [11] Hedvig Kjellström, Javier Romero, and Danica Kragić. Visual object-action recognition: Inferring object affordances from human demonstration. *Computer Vision and Image Understanding*, 115(1):81–90, 2011. 2
- [12] Mia Kokic, Danica Kragic, and Jeannette Bohg. Learning task-oriented grasping from human activity datasets. *IEEE Robotics and Automation Letters*, 5(2):3352–3359, 2020. 2
- [13] K Niranjana Kumar, Irfan Essa, Sehoon Ha, and C Karen Liu. Estimating mass distribution of articulated objects using non-prehensile manipulation. *arXiv preprint arXiv:1907.03964*, 2019. 3
- [14] Ian Lenz, Honglak Lee, and Ashutosh Saxena. Deep learning for detecting robotic grasps. *The International Journal of Robotics Research*, 34(4-5):705–724, 2015. 2, 3
- [15] Xueting Li, Sifei Liu, Kihwan Kim, Xiaolong Wang, Ming-Hsuan Yang, and Jan Kautz. Putting humans in a scene: Learning affordance in 3d indoor environments. In *IEEE Conference on Computer Vision and Pattern Recognition*, 2019. 3
- [16] Priyanka Mandikal and Kristen Grauman. Learning dexterous grasping with object-centric visual affordances. In *IEEE International Conference on Robotics and Automation (ICRA)*, 2021. 2, 3

- [17] Kaichun Mo, Leonidas J. Guibas, Mustafa Mukadam, Abhinav Gupta, and Shubham Tulsiani. Where2act: From pixels to actions for articulated 3d objects. In *Proceedings of the IEEE/CVF International Conference on Computer Vision (ICCV)*, pages 6813–6823, October 2021. [2](#), [3](#), [7](#), [8](#)
- [18] Kaichun Mo, Yuzhe Qin, Fanbo Xiang, Hao Su, and Leonidas Guibas. O2O-Afford: Annotation-free large-scale object-object affordance learning. In *Conference on Robot Learning (CoRL)*, 2021. [3](#)
- [19] Kaichun Mo, Shilin Zhu, Angel X. Chang, Li Yi, Subarna Tripathi, Leonidas J. Guibas, and Hao Su. PartNet: A large-scale benchmark for fine-grained and hierarchical part-level 3D object understanding. In *The IEEE Conference on Computer Vision and Pattern Recognition (CVPR)*, June 2019. [2](#), [7](#)
- [20] Tushar Nagarajan and Kristen Grauman. Learning affordance landscapes for interaction exploration in 3d environments. In *NeurIPS*, 2020. [2](#), [3](#)
- [21] NVIDIA. Nvidia.physx. [7](#)
- [22] L Peterson, David Austin, and Danica Kragic. High-level control of a mobile manipulator for door opening. In *Proceedings. 2000 IEEE/RSJ International Conference on Intelligent Robots and Systems (IROS 2000)(Cat. No. 00CH37113)*, volume 3, pages 2333–2338. IEEE, 2000. [1](#)
- [23] Charles R Qi, Li Yi, Hao Su, and Leonidas J Guibas. Pointnet++: Deep hierarchical feature learning on point sets in a metric space. *arXiv preprint arXiv:1706.02413*, 2017. [4](#)
- [24] William Qi, Ravi Teja Mullapudi, Saurabh Gupta, and Deva Ramanan. Learning to move with affordance maps. *arXiv preprint arXiv:2001.02364*, 2020. [3](#)
- [25] Yuzhe Qin, Rui Chen, Hao Zhu, Meng Song, Jing Xu, and Hao Su. S4g: Amodal single-view single-shot se (3) grasp detection in cluttered scenes. In *Conference on robot learning*, pages 53–65. PMLR, 2020. [2](#)
- [26] Zengyi Qin, Kuan Fang, Yuke Zhu, Li Fei-Fei, and Silvio Savarese. Keto: Learning keypoint representations for tool manipulation. In *2020 IEEE International Conference on Robotics and Automation (ICRA)*, pages 7278–7285. IEEE, 2020. [2](#), [3](#)
- [27] Kate Rakelly, Aurick Zhou, Chelsea Finn, Sergey Levine, and Deirdre Quillen. Efficient off-policy meta-reinforcement learning via probabilistic context variables. In *International conference on machine learning*, pages 5331–5340. PMLR, 2019. [3](#)
- [28] Joseph Redmon and Anelia Angelova. Real-time grasp detection using convolutional neural networks. In *2015 IEEE International Conference on Robotics and Automation (ICRA)*, pages 1316–1322. IEEE, 2015. [2](#), [3](#)
- [29] Tanner Schmidt, Richard A Newcombe, and Dieter Fox. Dart: Dense articulated real-time tracking. In *Robotics: Science and Systems*, volume 2. Berkeley, CA, 2014. [1](#)
- [30] Yu Sun, Shaogang Ren, and Yun Lin. Object-object interaction affordance learning. *Robotics and Autonomous Systems*, 62(4):487–496, 2014. [3](#)
- [31] Dimitrios Tzionas and Juergen Gall. Reconstructing articulated rigged models from rgb-d videos. In *European Conference on Computer Vision*, pages 620–633. Springer, 2016. [1](#)
- [32] Yusuke Urakami, Alec Hodgkinson, Casey Carlin, Randall Leu, Luca Rigazio, and Pieter Abbeel. Doorgym: A scalable door opening environment and baseline agent. *Deep RL workshop at NeurIPS 2019*, 2019. [1](#)
- [33] Xiaogang Wang, Bin Zhou, Yahao Shi, Xiaowu Chen, Qinpeng Zhao, and Kai Xu. Shape2motion: Joint analysis of motion parts and attributes from 3d shapes. In *Proceedings of the IEEE/CVF Conference on Computer Vision and Pattern Recognition*, pages 8876–8884, 2019. [1](#)
- [34] Yijia Weng, He Wang, Qiang Zhou, Yuzhe Qin, Yueqi Duan, Qingnan Fan, Baoquan Chen, Hao Su, and Leonidas J. Guibas. Captra: Category-level pose tracking for rigid and articulated objects from point clouds. In *Proceedings of the IEEE International Conference on Computer Vision (ICCV)*, pages 13209–13218, October 2021. [1](#)
- [35] Ruihai Wu, Yan Zhao, Kaichun Mo, Zizheng Guo, Yian Wang, Tianhao Wu, Qingnan Fan, Xuelin Chen, Leonidas Guibas, and Hao Dong. VAT-Mart: Learning visual action trajectory proposals for manipulating 3d articulated objects. 2021. [2](#)
- [36] Fanbo Xiang, Yuzhe Qin, Kaichun Mo, Yikuan Xia, Hao Zhu, Fangchen Liu, Minghua Liu, Hanxiao Jiang, Yifu Yuan, He Wang, Li Yi, Angel X. Chang, Leonidas J. Guibas, and Hao Su. SAPIEN: A simulated part-based interactive environment. In *The IEEE Conference on Computer Vision and Pattern Recognition (CVPR)*, June 2020. [2](#), [7](#)
- [37] Zhenjia Xu, Jiajun Wu, Andy Zeng, Joshua B Tenenbaum, and Shuran Song. Densphysnet: Learning dense physical object representations via multi-step dynamic interactions. *arXiv preprint arXiv:1906.03853*, 2019. [3](#)
- [38] Zhihao Yan, Ruizhen Hu, Xingguang Yan, Luanmin Chen, Oliver van Kaick, Hao Zhang, and Hui Huang. RPM-NET: Recurrent prediction of motion and parts from point cloud. *ACM Trans. on Graphics*, 38(6):Article 240, 2019. [1](#)
- [39] Lixin Yang, Xinyu Zhan, Kailin Li, Wenqiang Xu, Jiefeng Li, and Cewu Lu. Cpf: Learning a contact potential field to model the hand-object interaction. In *Proceedings of the IEEE/CVF International Conference on Computer Vision*, pages 11097–11106, 2021. [2](#)
- [40] Li Yi, Haibin Huang, Difan Liu, Evangelos Kalogerakis, Hao Su, and Leonidas Guibas. Deep part induction from articulated object pairs. *ACM Trans. Graph.*, 37(6), Dec. 2018. [1](#)
- [41] Wenhao Yu, Jie Tan, C Karen Liu, and Greg Turk. Preparing for the unknown: Learning a universal policy with online system identification. *arXiv preprint arXiv:1702.02453*, 2017. [3](#)
- [42] Tony Z Zhao, Anusha Nagabandi, Kate Rakelly, Chelsea Finn, and Sergey Levine. Meld: Meta-reinforcement learning from images via latent state models. *arXiv preprint arXiv:2010.13957*, 2020. [3](#)
- [43] Wenxuan Zhou, Lerrel Pinto, and Abhinav Gupta. Environment probing interaction policies. In *7th International Conference on Learning Representations, ICLR 2019, New Orleans, LA, USA, May 6-9, 2019*. OpenReview.net, 2019. [3](#)
- [44] Yixin Zhu, Yibiao Zhao, and Song Chun Zhu. Understanding tools: Task-oriented object modeling, learning and recogni-

8. More Detailed Data Statistics

Table 3 summarizes the data statistics and splits.

Figure 6 visualizes some example shapes from our dataset.

9. Ablation Study

Besides the two baselines in our main paper, we further compare our method with an ablated version. The ablated version is the method that removes the attention module in Adaptive Information Encoder of our AdaAfford framework. In other words, different interactions from the interactions set \mathcal{I} weigh equally in the summarized hidden information $z_{\mathcal{I}}$. Table 2 shows that our method outperforms the ablated version in most comparison entries.

10. More Results and Analysis

In Figure 7 and 8, we show more qualitative results. See the captions of these two figures for more details.

		F-score (%)	Sample-Succ (%)
pushing all (train cat.)	ours-w/o attention	69.61/68.84/69.49	32.84/35.00/34.05
	ours-final	70.50 / 73.96 / 74.63	35.70 / 35.50 / 35.14
pushing all (test cat.)	ours-w/o attention	49.26/52.31/53.60	27.53/32.08/31.94
	ours-final	58.44 / 58.06 / 60.38	30.00 / 30.39 / 33.50
pulling all (train cat.)	ours-w/o attention	35.84/34.77/34.63	1.88/2.81/4.96
	ours-final	35.73 / 37.20 / 37.50	3.33 / 6.67 / 9.44
pulling all (test cat.)	ours-w/o attention	38.25/39.01/39.58	4.70/2.94/2.65
	ours-final	39.10 / 35.29 / 49.78	10.45 / 10.83 / 10.87
pulling closed door	ours-w/o attention	49.69/51.40/50.24	9.66/8.49/15.58
	ours-final	56.11 / 58.68 / 67.68	7.63 / 11.36 / 17.08
pushing faucet	ours-w/o attention	72.59/72.52/69.03	32.61/31.71/37.81
	ours-final	76.01 / 76.93 / 78.40	36.53 / 46.23 / 50.44

Table 2. **Quantitative Evaluations and Comparisons.** We compare our method with the “ours-w/o attention” approach that removes the attention score in Adaptive Information Encoder. We experiment with three different test-time interaction budgets (*i.e.*, 1, 2, or 4) and report the numbers separated by slashes. We use “pushing all” and “pulling all” to denote the experiments over all object categories, while “pulling closed door” and “pushing faucet” refer to the experiments over a single category only. For the experiments over all categories, we report the performance over novel shapes from the training categories (marked with “train cat.”) and shapes from novel categories (marked with “test cat.”). We see clearly that ours-final achieves the best performance in most comparison entries.

Train-Cats	Box	Microwave	Door	Faucet	TrashCan
Train / Test	20 / 8	9 / 3	23 / 12	65 / 19	52 / 17
	Kettle	Refrigerator	Switch	Cabinet	Window
	22 / 7	32 / 11	53 / 17	270 / 75	40 / 18
Total	586 / 187				
Test-Cats	Table	Washer	Bucket	Pot	Safe
	95	16	36	23	29
Total	199				
ADDL Exp.	Category	Train data	Test data		
Closed door	Cabinet	74	11		
Faucet	Faucet	15	4		

Table 3. We first summarize the shape counts in our dataset for pushing and pulling shapes over all categories, in which there are three data splits: training data from the training categories, test data from the training categories, and data from the test categories. We use the first split to train and use the rest two for evaluation. We further show the shape counts in our two additional tasks: pulling closed door and pushing faucet (denoted as Closed Door and Faucet for brevity).



Figure 6. **Data Visualization.** We show example shapes of object categories in our paper.

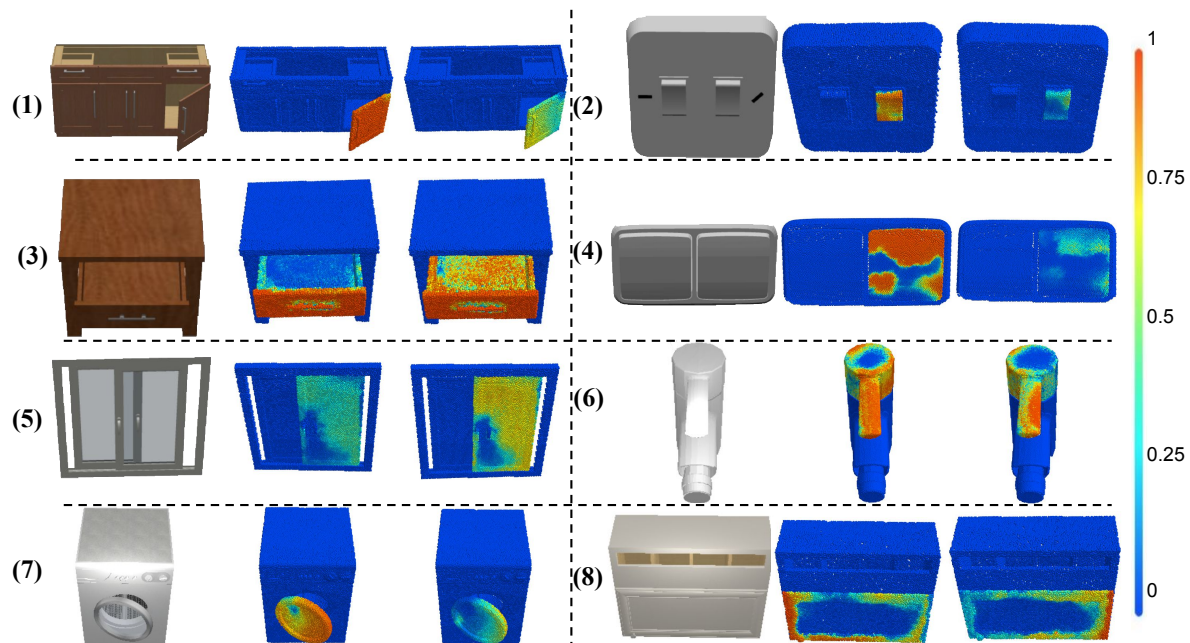


Figure 7. We visualize more results for the adapted affordance predictions given by the AAP module conditioned on different hidden kinematic and dynamic information. From the first to the last block, we respectively change the 1) mass of target part 2) joint friction 3) friction coefficient on the target part's surface 4) joint friction 5) friction coefficient on the target part's surface 6) rotating direction of the faucet 7) mass of target part 8) axis location of the door, and clearly see reasonable adaptations in affordance predictions.

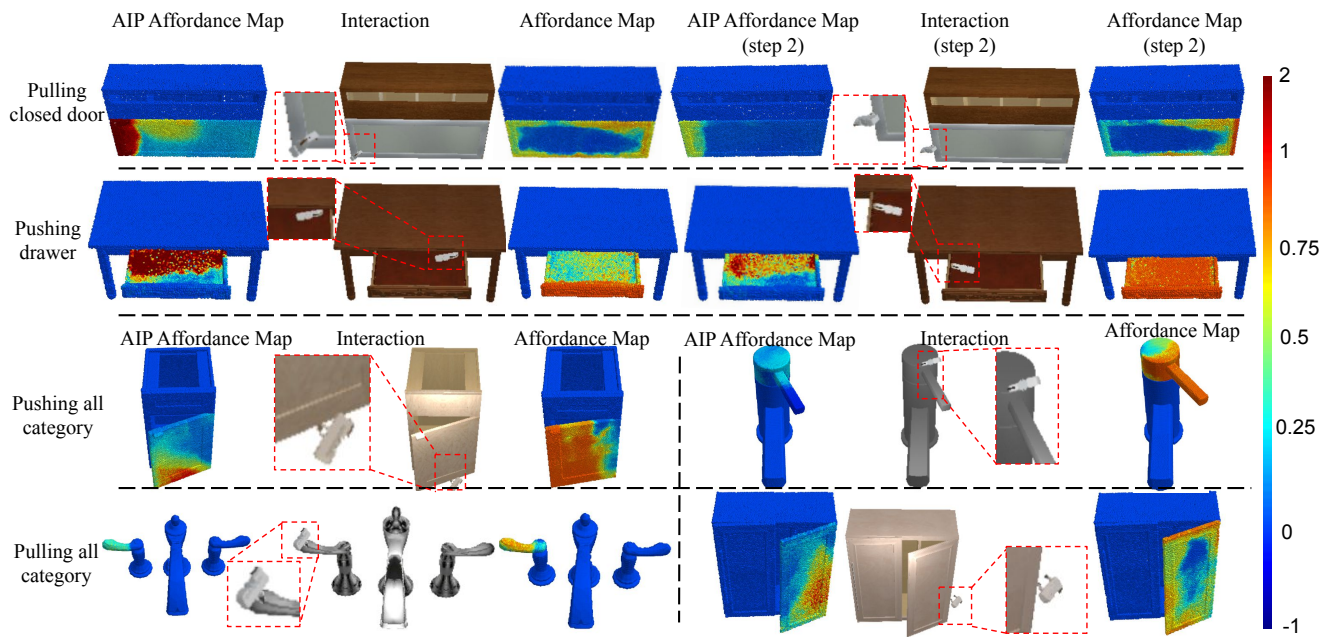


Figure 8. We visualize more results for the interactions proposed by the AIP module and the corresponding AIP affordance map predictions. In the first two rows, we show the initial and the second AIP affordance maps, the corresponding proposed interactions, and the posterior affordance map predictions. In the third and fourth rows, we present four more examples that only one interaction is needed. From these results, we observe that our AIP module successfully proposes reasonable interactions for querying useful hidden information.